Manganese in Precipitated Hydroxyapatites

Isaac Mayer,*[a] Orit Jacobsohn,[a] Tamara Niazov,[a] Jacques Werckmann,[b] Monica Iliescu,[b] Mireille Richard-Plouet,[b] Olaf Burghaus,[c] and Dirk Reinen[c]

Keywords: Manganese / Hydroxyapatite / EPR spectroscopy / Thermal properties

The synthesis of Mn-containing hydroxyapatite (HA) samples was carried out by precipitation from an aqueous solution with and without carbonate at pH 5.8–6.0. Chemical analyses have shown that Mn uptake (about 70%) is proportional to the amount of initially added Mn. The molar Ca/P ratios of the samples (1.53–1.63) indicate the formation of nonstoichiometric HA, with the higher values being obtained for the carbonated samples. Powder X-ray diffraction (XRD) and IR spectroscopy have shown well-defined patterns with structural data characteristic of HA. The calculated lattice constants were found to be similar to those known for HA, without any effect of the varying Mn content. High temperature treatment of selected samples was studied by XRD and IR and showed that the apatite structure is stable up to 400 °C for all samples. At 600 °C samples with low carbonate content transform partially, and at 800 °C completely, to β-$Ca_3(PO_4)_2$, while for samples with higher carbonate content (3.5–6.0%) the apatite structure is stable up to 800 °C, and a colour change to blue occurs. EPR spectroscopy reveals that manganese is divalent in all precipitated samples and present in a cubic impurity phase. After heating above 600 °C it is partially oxidized to Mn^V in the samples with high carbonate content and enters the HA lattice as the blue MnO_4^{3-} ion. In the carbonate-poor solids Mn^{2+} seems to partly occupy the Ca^{2+} sites in β-$Ca_3(PO_4)_2$ when sintered at temperatures above 400 °C.

Introduction

Various calcium hydroxyapatites (HA) containing Mn^{2+} ions were prepared in the course of a project dealing with the surface improvement of metal implants. HA is frequently used in implant materials for orthopaedic applications because of its biocompatibility. The addition of Mn^{2+} ions to HA in the present work was due to the fact that divalent Mn^{2+} has been linked to the activation of integrins,[1] a family of receptors which mediate cellular interactions with extracellular matrix and cell-surface ligands. In the presence of Mn^{2+} ions the ligand affinity of integrin increases and cell adhesion is promoted.

It is well-known that Mn^{2+} may enter the divalent M^{II} metal positions of apatites at the doping level, preferentially the M(I) site on a C_3 axis and with the coordination number 9 with respect to oxygen. The EPR spectra of Mn^{2+} in the Ca(I) position of the fluoride apatite $Ca_5(PO_4)_3F$ have been reported, indicating an axial lower-symmetry ligand field according to a zero-field splitting, D, of 428 G (about four times larger than the hyperfine splitting A).[2] Single crystal spectra of Mn^{2+}-doped $Cd_5(PO_4)_3Cl$ yield rather similar values ($D \approx 457$ G; $A \approx 92$ G).[3] Manganese may also enter the tetrahedral positions in the (+V) oxidation state, however, and a series of detailed single-crystal and powder studies centred on the optical and EPR properties have been published.[4]

Results

Chemical Analyses

Table 1 is a partial list of the analytical results of the synthesised samples (for preparation see Exp. Sect.). The molar Ca/P ratios found were in the range of 1.51−1.62, lower than the ratio for stoichiometric HA (1.67), thus indicating that under the experimental conditions used nonstoichiometric HA is obtained. Higher values of Ca/P are usually obtained for carbonate-containing samples. The Mn contents found in the samples were proportional to the initial amounts of Mn ions added and were about 70% of the original percentages.

Crystal Phase Analyses

Powder XRD patterns of the samples consisted of well defined reflections with the characteristic $P6_3/m$ hexagonal structure of apatites and with no additional crystal phases. The calculated lattice constants are listed in Table 1, and

[a] Department of Inorganic & Analytical Chemistry, Hebrew University, 91904 Jerusalem, Israel
[b] IPCMS, Universite Louis Pasteur, Strasbourg, France
[c] Fachbereich Chemie and Zentrum für Materialwissenschaften, Philipps Universität, 35032 Marburg, Germany

Table 1. Hydroxyapatite samples with different amounts of carbonate and Mn Lattice constants and Ca/P values

Sample	Mn^{2+} added (mg)	Mn^{2+} found (%)	CO_3^{2-} added (mL)	CO_3^{2-} found (%)	Lattice constants a (Å)	c (Å)	Ca/P
HAMn20	12.1	0.28	–	2.4	9.397	6.862	1.61
HAMn21	24.2	0.54	–	–	9.397	6.862	1.65
HAMn19	36.2	0.74	–	1.3	9.391	6.846	1.62
HAMn18	48.3	1.08	–		9.397	6.862	1.62
HAMn25	12.1	0.27	10	0.9	9.423	6.871	1.57
HAMn22	24.2	0.55	10	0.9	9.402	6.846	1.53
HAMn24	36.2	0.80	10	–	9.439	6.871	1.51
HAMn23	12.1	0.25	5	2.3	9.407	6.871	1.58
HAMn28	24.2	0.55	5	2.8	9.423	6.862	1.54
HAMn53	8.8	0.17	–	1.8	9.410	6.868	1.61
HAMn52	17.5	0.33	–	3.2	9.394	6.852	1.59
HAMn51	26.2	0.52	–		9.376	6.854	1.59
HAMn50	35.0	0.68	–	1.9	9.391	6.862	1.55
HAMn57	8.8	0.15	10	5.0	9.421	6.882	1.60
HAMn56	17.5	0.33	10	4.0	9.414	6.873	1.63
HAMn55	26.2	0.47	10	3.6	9.412	6.868	1.63
HAMn54	35.0	0.66	10	3.3	9.407	6.862	1.60
HAMn58	–	–	–	1.6	9.410	6.862	1.59
HAMn59	–	–	10	4.0	9.412	6.879	1.61
HAMn60	26.2	0.52	–	1.2	9.381	6.854	1.61
HAMn65	26.2	0.45	–	1.1	9.407	6.865	1.58
HAMn61	26.2	0.44	10	2.6	9.428	6.884	1.61
HAMn63	17.5	0.29	–	1.2	9.409	6.869	1.59
HAMn69	8.8	0.14	15	5.9	9.391	6.829	1.63
HAMn66	17.5	0.30	15	3.0	9.414	6.877	1.62
HAMn62	26.2	0.45	15	2.8	9.410	6.873	1.62
HAMn68	35.0	0.72	15	4.4	9.422	6.886	1.62

are close to those of pure HA. The amount of Mn added during precipitation has no apparent effect on the lattice constant values.

The IR spectra of the samples display the characteristic phosphate, hydroxide and water bands of HA. The carbonate bands appear around 1420 and 1470 cm^{-1}, indicating the replacement of phosphate by carbonate (B-type). In samples without carbonate HPO_4^{2-} could be detected by a band at around 866 cm^{-1}.

Thermal Properties

The thermal properties of selected samples were studied by heating them during four hours in the temperature range of 400−800 °C in 200 °C intervals. The samples were then analysed by XRD. The results of this thermal treatment are summarised in Table 2. The XRD patterns of the samples heated up to 800 °C display very sharp and well-defined peaks, an indication of improved crystallinity. The samples show no change in their crystal structure after heating up to 400 °C, and only one crystal phase − the apatite structure − is present. At 600 °C the apatite structure is still the only crystal phase found for the samples containing more than 4% carbonate. The XRD powder patterns of all the other samples have, in addition to the apatite phase, the diffraction peaks of β-$Ca_3(PO_4)_2$ (β-TCP),[5] indicating the partial transformation of HA to β-TCP. At 800 °C samples without, or with up to 2%, carbonate transform almost completely to β-TCP. The samples with a carbonate content equal to or higher than 4% do not decompose at all during thermal treatment but their colour turns to blue above 600 °C. This colour change is most pronounced in samples with low Mn content (around 0.1%); above 1.0% Mn, part of the crystallites are brownish. No such colour changes were observed for the samples which transform to β-TCP.

EPR Spectroscopy

Figure 1 shows the Q-band spectrum and the second derivative of a sample after precipitation and drying. The spectrum is characteristic of Mn^{2+} in a cubic environment, with a well-resolved sextet due to the hyperfine interaction with the manganese nucleus. A significant zero- field splitting, indicating lower-symmetry crystal field components − which should be observable if Mn^{2+} substitutes into the Ca^{2+} position of the apatite lattice[3] − cannot be detected. Apparently, Mn^{2+} is present as an impurity phase (oxidic or hydroxy), sometimes with manganese clustering, which shows up in an only partly resolved hyperfine structure of many samples.

Annealing at 400 °C leads already to distinct changes in the environment of part of the Mn^{2+} ions, obviously induced by the onset of migration of manganese into the apatite lattice. This is deduced from the Q-band spectrum in Figure 2 (top), for example, where new lines beside the original sextet appear, but even more distinctly in the X-band region, where more or less pronounced additional absorptions, in particular at lower magnetic fields, supplement the original broad signal around 3300 G (Figure 2; bottom). However, more precise information is obtained by looking

Table 2. Mn-containing HA samples heated at temperatures above 400 °C; structure stability and colour changes are indicated

Sample	600 °C	800 °C	Mn (%)	CO_3 (%)	600 °C	800 °C
HAMn20		Transf.	0.56	–		white
HAMn28		Transf.	0.52	2.8		white
HAMn56	Minor Transf.	No Transf.	0.33	4.0	light grey	blue grey
HAMn52	Partial Transf.	Partial Transf.	0.33	3.2	white	light grey
HAMn64	Minor Transf.	Partial Transf.	–	1.2	white	white
HAMn54		Partial Transf.	0.66	3.3		light grey
HAMn57	No Transf.	No Transf.	0.15	5.0	light blue	blue grey
HAMn68	Minor Transf.	No Transf.	0.72	4.4	grey	grey
HAMn69	No Transf.	No Transf.	0.19	5.9	blue	blue
HAMn50	Partial Transf.	Transf.	0.68	1.9	white	light grey
HAMn55		Minor Transf.	0.47	3.6		light grey
HAMn61		Minor Transf.	0.41	2.6		light grey
HAMn65		Partial Transf.	0.45	1.1		light grey
HAMn75	Minor Transf.	Minor Transf.	0.70	3.6	blue	blue grey
HAMn73	Minor Transf.	Minor Transf.	0.30	3.6	white	blue
HAMn77	Partial Transf.	Partial Transf.	0.59	2.6	light blue	grey
HAMn83	No Transf.	No Transf.	0.30	4.2	light blue	blue grey
HAMn86	No Transf.	Partial Transf.	0.17	1.0	white	white

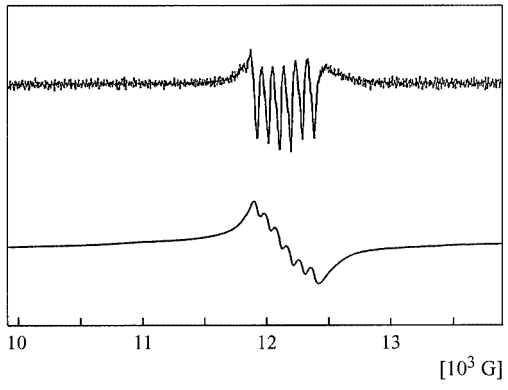

Figure 1. Q-band spectrum of the non heated sample HAMn61 (33.99 GHz, 298 K); the second derivative spectrum is also shown (above)

at the EPR spectra samples after heat treatment at 600 °C and 800 °C. The Q-band spectrum in Figure 3 depicts the typical situation for compounds with vanishingly small or very low CO_3^{2-} contents, which transform to β-TCP when heated to higher temperatures. This spectrum is typical for zero-field effects, displaying a centrosymmetric intensity distribution; the fine structure transitions are broad and not resolved into hyperfine sextets, except in the central part. The optical spectra give no evidence for oxidation states of manganese beyond +II, in agreement with the white colour. A moderate zero-field splitting *D* of about 500 G is estimated, which is near to the value for Mn^{2+} doped into the Cd^{2+} position of the $Cd_5(PO_4)_3Cl$ apatite.[3] One can easily follow this argument by direct comparison. The group of lines five (I–V) due to the zero-field splitting, which is induced by the non-cubic ligand-field component, are each nicely resolved into the six hyperfine components in the case of Mn^{2+}-doped $Cd_5(PO_4)_3Cl$ (powdered single crystals); they are also present in the β-TCP sample, however, as broad absorptions — presumably because of Mn^{2+} clustering in the host. We therefore conclude that Mn^{2+} has partly entered one of the five Ca^{2+} positions in β-TCP – presumably Ca(5) with a pseudo-octahedral coordination.[6]

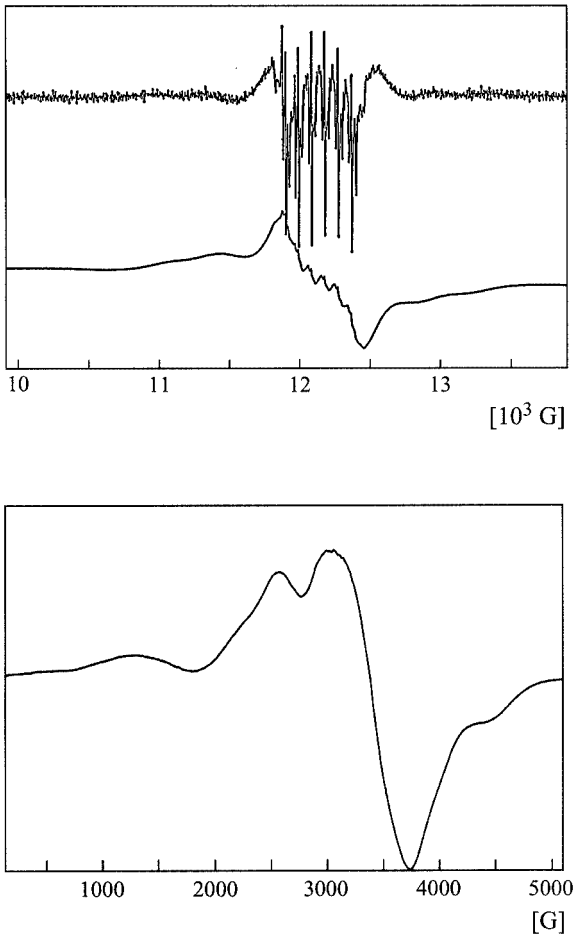

Figure 2. Q-band spectrum and second derivative of sample HAMn21, annealed at 400 °C (33.98 GHz, 298 K; top) and X-band spectrum of the same sample (9.23 GHz, 120 K; bottom)

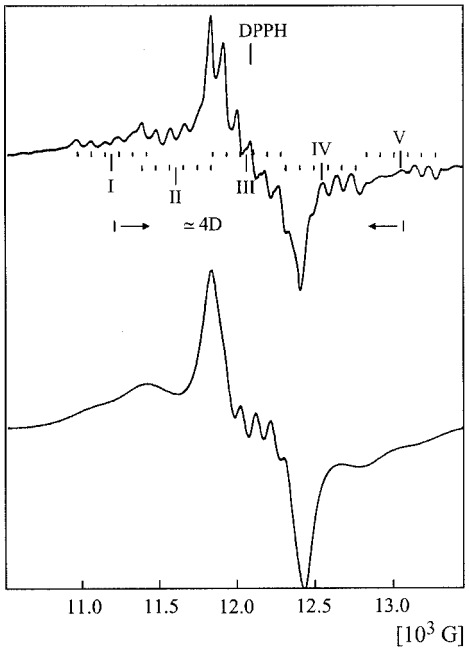

Figure 3. Q-band spectrum of sample HAMn28 with low carbonate content and annealed at 800 °C (33.98 GHz, 298 K; bottom) in comparison with the Q-band spectrum of Mn^{2+}-doped $Cd_5(PO_4)_3Cl$ (adapted from ref.;[3] top)

A different situation arises when looking at the samples with higher carbonate content, heated to temperatures above 400 °C. They turn bluish and the optical spectra indicate $Mn^{V}O_4$ tetrahedra; the split and intensity-dominating $^3A_2(e^2) \rightarrow {}^3T_1(\approx e^1t_2^1)$ transition shows the same structure and appears at the same energy (Figure 4) as the colour-determining band of Mn^{V}-doped apatites synthesised by high-temperature solid-state reactions.[7a,7b] Correspondingly, a diverse spectral intensity distribution becomes apparent in the EPR spectra, with a considerably larger fine

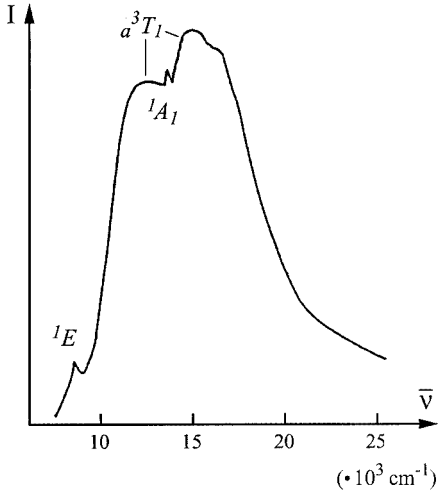

Figure 4. The optical powder reflection spectrum of sample HAMn69, heated at 800 °C, between 8000 and 28000 cm^{-1}; besides the allowed $^3A_2 \rightarrow {}^3_aT_1$ band around 12000 to 15000 cm^{-1} the characteristic narrow spin-forbidden transitions $^3A_2 \rightarrow {}^1E$, $^1A_1$ within the e^2 ground-state configuration are seen at 8700 and 13500 cm^{-1}, respectively

structure splitting. This is particularly observable in the X-band spectra, where signal groups extend down to 700 G, in contrast to the former case with low carbonate content (Figure 5). The described features roughly correspond to those typical for tetrahedral Mn^{V} in apatites.[7a] Apparently part of the manganese present has been oxidized and has entered the apatite lattice. A reaction where CO_3^{2-} is positioned on a PO_4^{3-} lattice position and OH^- is a constituent of the apatite host [depicted in Equation (1)] would offer an explanation for these spectral findings.

$$Mn^{II}(OH)_2 + CO_3^{2-} + OH^- + 3/4O_2 \rightarrow Mn^{V}O_4^{3-} + CO_2 + 3/2H_2O \quad (1)$$

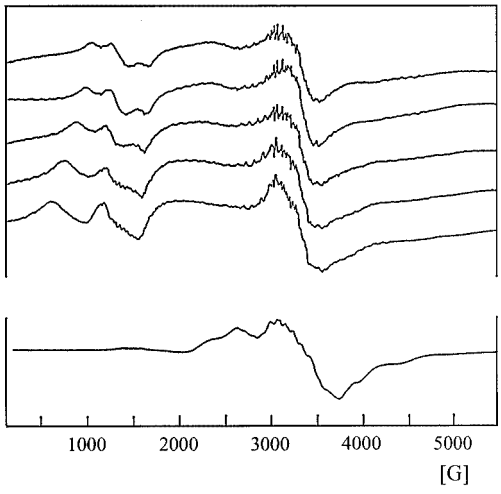

Figure 5. X-band spectra (9.21 GHz) of sample HAMn69, after heating to 800 °C, at temperatures 340, 293, 280, 170 and 117 K (above) and of sample HAMn86 (below), after heating to 800 °C, at 298 K

EDX Analysis and TEM Electron Microscopy

The results of the EDX analysis of two representative samples, HAMn23 and HAMn61, are shown in Figure 6 and 7. The Ca/P ratios and the Mn content obtained at different locations within the samples show that the Ca/P ratio is relatively constant, while Mn is not homogeneously dispersed in the samples.

The results of the TEM analysis of selected samples have shown that in the samples with and without carbonate and with Mn, crystals appear in the form of sticks and platelets. Figure 8 and 9 are TEM pictures of samples HAMn2 (no CO_3, 0.56% Mn) and HAMn61 (2.6% CO_3, 0.44% Mn). Sticks and plates appear in both and in the case of HaMn61 fibres can also be seen. In Figure 9 (sample HAMn59) wider sticks and plates appear, but no fibres are present, which indicates that Mn may play a role in the formation of fibres. The main morphological observations obtained are summarised in Table 3.

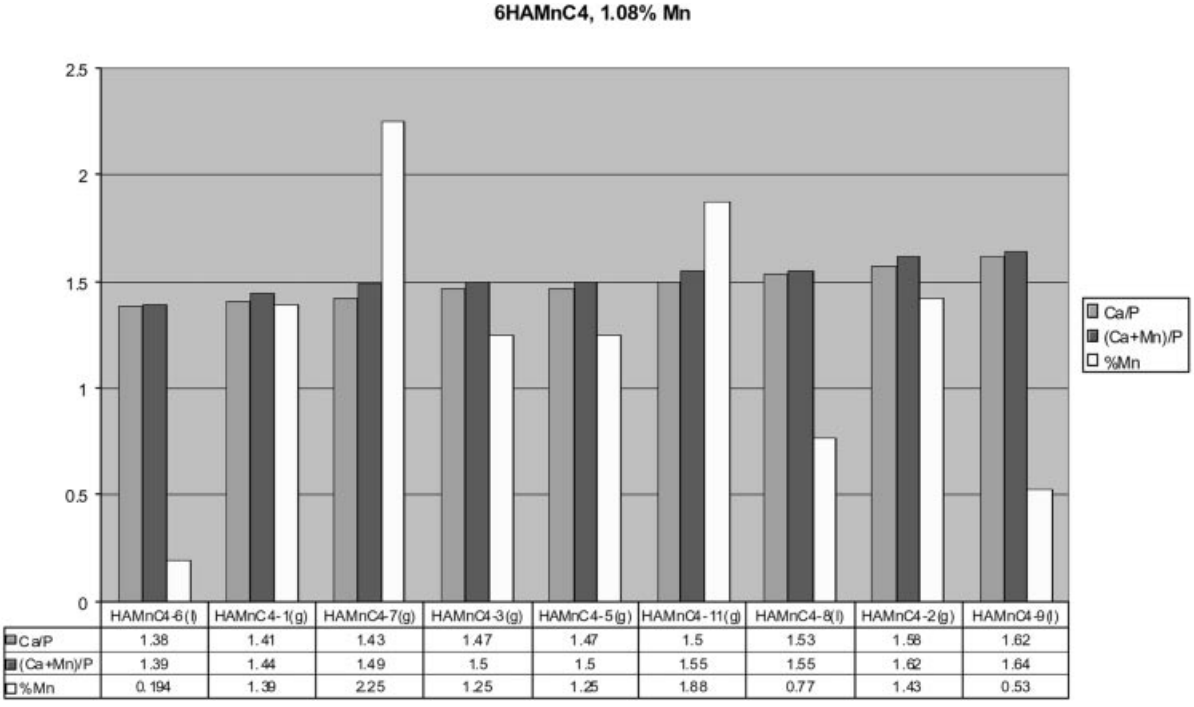

	HAMnC4-6(l)	HAMnC4-1(g)	HAMnC4-7(g)	HAMnC4-3(g)	HAMnC4-5(g)	HAMnC4-11(g)	HAMnC4-8(l)	HAMnC4-2(g)	HAMnC4-9(l)
Ca/P	1.38	1.41	1.43	1.47	1.47	1.5	1.53	1.58	1.62
(Ca+Mn)/P	1.39	1.44	1.49	1.5	1.5	1.55	1.55	1.62	1.64
%Mn	0.194	1.39	2.25	1.25	1.25	1.88	0.77	1.43	0.53

Figure 6. EDX analysis results of sample HAMn23

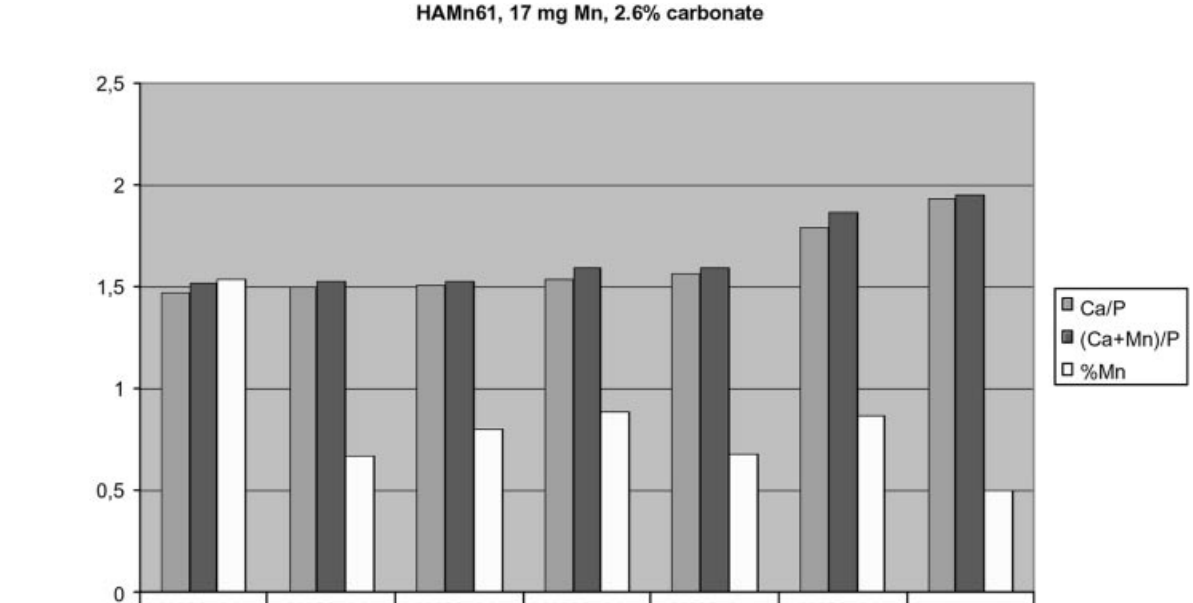

	HAMn61-4(g)	HAMn61-1(g)	HAMn61-5(g)	HAMn61-3(g)	HAMn61-2(g)	HAMn61-6(p)	HAMn61-7(f)
Ca/P	1,47	1,5	1,51	1,54	1,57	1,79	1,93
(Ca+Mn)/P	1,52	1,53	1,53	1,6	1,6	1,87	1,95
%Mn	1,54	0,67	0,8	0,89	0,68	0,87	0,5

Figure 7. EDX analysis results of sample HAMn 61

Discussion

The main aim of this work was to prepare precipitated HA samples in the presence of Mn^{2+} and to investigate their properties. The analytical data concerning the chemical composition of the samples, as well as their XRD and FTIR data, prove that apatite-type HA samples were obtained with their typical structural characteristics. The non-stochiometry of the samples, with molar Ca/P ratios of less than 1.67, is most probably due to the presence of HPO_4^{2-}

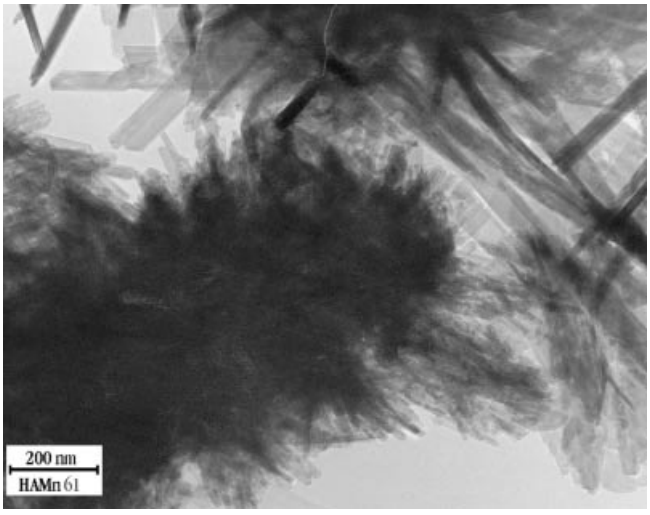

Figure 8. TEM picture of sample HAMn61

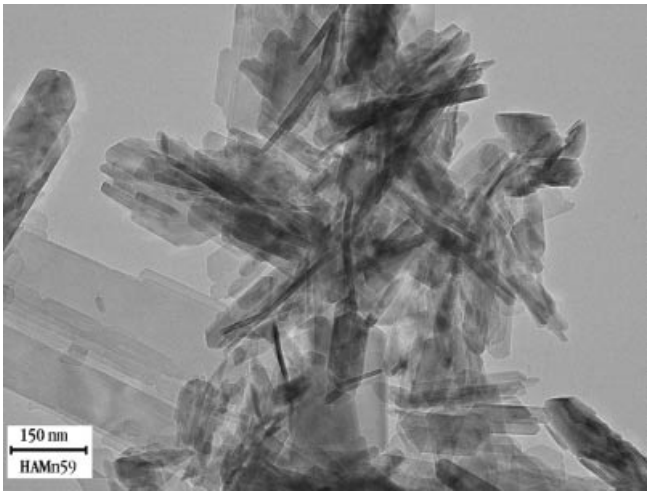

Figure 9. TEM picture of sample HAMn59

Table 3. Morphological data of various Mn-containing HA samples; l: length; w: width; e: thickness

Sample	CO_3 (%)	Mn (%)	Platelets (nm)	Fibers (nm)	Sticks (nm)
HAMn2	–	0.56	$w < 200$	–	$l < 500$; $e < 6$
HAMn4	–	1.08	$w < 200$	–	$l < 500$; $e \approx 10$
HAMnC2	0.9	0.55	$w < 120$	$l > 2\mu$; $e < 10$	
HAMnC4	–	1.08	$w < 150$	$l > 1\mu$; $e < 10$	
HAMnC6	2.6	0.54	$w < 100$	–	$l < 1\mu$; $e < 10$
HAMn65	1.1	0.45	$w < 250$	–	$l < 300$; $e < 10$
HAMn58	1.6	–	$l < 600$	–	
HAMn59	4.6	–	$l < 600$, $w < 150$	–	$l < 500$; $e < 10$

ions which occupy a small part of the anion sites of the compounds together with the PO_4^{3-} ions. Such an assumption is in good agreement with the structural and spectroscopic findings discussed below. The Ca/P ratios found by EDX analysis locally, and by global analyses as well, are close to the chemical analysis results. EPR spectroscopy shows that Mn is in the divalent state in all the samples. Mn^{2+} is present as a cubic (oxidic or hydroxy) impurity phase, which is not homogeneously distributed over the samples, as is clearly indicated by EDX analysis and also suggested by EPR spectroscopy.

TEM observations have shown that the morphology of the crystals is that of platelets, sticks and fibres. Platelets and sticks have also been found in HA samples precipitated in the presence of Zn[8] and Al.[9] In the present work fibre-like crystals were also observed. Apparently, further studies are needed to determine the role of Mn in the formation of fibre-type crystals.

Two types of high temperature behaviour have been observed: HA samples without or with carbonate contents up to about 3.5% transform partially or completely above 600 °C to β-TCP; samples with carbonate contents higher than 4% retain the apatite structure and their colour changes to blue above 600 °C. There is definite spectroscopic evidence that $Mn^{V}O_4^{3-}$ ions – generated by oxidation of Mn^{2+} and presumably substituting CO_3^{2-} ($+OH^-$) [cf. Equation (1)] in the HA structure – are responsible for this colour. In contrast manganese in the samples with low carbonate content remain in the (+II) oxidation state and partly migrate into Ca^{2+} positions of β-TCP and of HA as well, when heated to temperatures from 400 °C to 800 °C.

The simultaneous effect of $HPO_4^{2-}$and CO_3^{2-} ions on the thermal transformation of HA to β-TCP was discussed in a previous work[10] and it was shown that HPO_4^{2-} ions support this transformation; the CO_3^{2-} ions in carbonate-containing apatites prevent the incorporation of HPO_4^{2-} ions. The assumption of HPO_4^{2-} substituting PO_4^{3-} in the apatite lattice as the cause of the lower molar Ca/P ratios is well in agreement with the high temperature properties of precipitated HA samples. As Equation (2) indicates for an extreme case the presence of vacancies in the Ca^{2+} sublattice and the release of water on heating – which leaves the OH^- positions unoccupied – destabilizes the apatite structure and favours the structural transformation to β-TCP. Indeed, such a transformation is often observed for HA samples with small molar Ca/P ratios. On the other hand, the presence of larger amounts of carbonate, which is known to replace phosphate in HA to a certain extent, prevents the formation of β-TCP on annealing,[10] as Equation (3) – again for an extreme case – illustrates nicely.

$$\square_{0.5}Ca_{4.5}(PO_4)_2(HPO_4)OH \rightarrow 1.5\,Ca_3(PO_4)_2 + H_2O \quad (2)$$

$$\square_{0.5}Ca_{4.5}(PO_4)_2(HPO_4)_{0.7}(CO_3)_{0.3}OH \rightarrow 0.9Ca_5(PO_4)_3OH + 0.3CO_2 + 0{\cdot}4H_2O \quad (3)$$

It is clearly the basic character of CO_3^{2-} that stabilizes the apatite lattice, as well as the fact that the substitution of PO_4^{3-} by CO_3^{2-} in the lattice raises the Ca/P ratio towards that characteristic for stoichiometric apatite (Table 1). The basic (O^{2-} donor) properties of CO_3^{2-} are

also needed for the oxidation from Mn^{II} to Mn^{V} [Equation (1)]. If the manganese concentration becomes too high, such an oxidation process is only partly possible; most of the manganese is oxidized to Mn^{IV} in that case − where O^{2-} donors are not needed − as indicated by the brownish colour (MnO_2 impurities).

In a very recent EPR study[11] it was suggested that in precipitated HA (carbonate-free, manganese presence), heated to 400 °C, Mn^{2+} has partly migrated into the Ca^{2+} position − in perfect agreement with the results presented here.

Experimental Section

Sample Preparation and Characterisation

Samples of HA with Mn (0.1−2.0%), and with (1.0−6.0%) and without carbonate, were prepared by a precipitation method described in more detail elsewhere.[12] A phosphate solution [3.7 g of $(NH_4)_2HPO_4$ in 200 mL of triply distilled water (TDW)] was added dropwise to a calcium solution [9.47 g $Ca(NO_3)_2{\cdot}4H_2O$ in 200 mL TDW]. Carbonate was added [5.0, 10.0, 15.0 and 20.0 mL] from a 1 M $NaHCO_3$ stock solution. These additions were designed to give 2.5−3.5 and 3.5−6.0% carbonate in the final sample. The amount of Mn added was 0, 2.5, 5.0, 10, 15.0, 20.0 and 25.0 mL per sample from a 0.025 M $MnCl_2$ solution.

For the preparation of HA samples with Mn^{2+} the pH of 5.8−6.0 was chosen because it was found that at this pH Mn^{2+} is not oxidized to a higher valence state. The pH was maintained constant during precipitation by adding NaOH solution using a Mettler pH-stat automatic titrator. The precipitation was carried out during 2 h, and following this the temperature was raised to boiling point and the system was refluxed for 2 h. The sample was then washed with TDW and dried overnight in air at 120 °C.

The Ca, P and Mn contents of the samples were determined by ICP-atomic emission spectroscopy with a precision of ±0.1, ±0.5, and ±0.3% for Ca, P and Mn respectively.

Powder X-ray Diffraction (XRD) was used for crystal phase and lattice constant determination. The X-ray diffraction analyses were made by a Philips Automatic Diffractometer using Cu-K_α radiation. The samples were scanned in the 2θ range of 20−55°. The lattice parameters were calculated by a least-square computer program. The maximum deviation of the lattice constants was ±0.003 Å.

The characterisation of the samples by infrared spectroscopy (IR) was performed by a Nicolet FTIR spectrometer. Samples of approx. 1 mg were pressed into pellets with approx. 150 mg KBr. The carbonate content of the samples was estimated by IR analysis using the extinction ratio of the carbonate (1420 cm^{-1}) and phosphate (575 cm^{-1}) bands. Carbonate is determined by this method with an accuracy of ±5%.[13]

Thermal analyses of selected samples were carried out by heating in porcelain crucibles up to 800 °C in an electric furnace.

EPR measurements were performed at X- and Q-band frequencies between 300 and 80 K with a Bruker ESP-300 spectrometer. UV/Vis spectra were recorded using the powder diffuse-reflection technique with a Zeiss PMQII spectrometer.

Samples were also examined by EDX analysis and by TEM electron microscopy. For this purpose they were ground and sonicated in ethanol. The thus-obtained suspension was deposited onto a carbon-coated grid. In local analysis of the samples the beam diameter was 18 nm, in global analysis 15 μ and 56 and 700 nm.

Acknowledgments

This work was supported by a grant from the European Union SIMI Contract G5RD-CT.

[1] A. Armulik, G. Svineng, K. Wennerberg, R. Faessler, S. Johansson, *Experimental Cell Res.* **2000**, *254*, 55−63.
[2] P. H. Kasai, *J. Phys. Chem.* **1962**, *66*, 674.
[3] I. Mayer, H. Diab, D. Reinen, Ch. Albrecht, *J. Mater. Sci.* **1993**, *28*, 2428−2432.
[4] D. Reinen, W. Rauw, U. Kesper, M. Atanasov, H. U. Gûdel, M. Hazenkamp, U. Oetliker, *J. Alloys Comp.* **1997**, *246*, 193−208, and references cited therein.
[5] *International Centre for Diffraction Data*. Powder Diffraction File, 09-0169, **2001**.
[6] B. Dickens, L. W. Schroeder, W. E. Brown, *J. Solid State Chem.* **1974**, *10*, 232−248.
[7] [7a] D. Reinen, H. Lachwa, R. Allmann, *Z. Anorg. Allg. Chem.* **1986**, *542*, 71−88. [7b] H. Lachwa, D. Reinen, *Inorg. Chem.* **1989**, *28*, 1044−1053.
[8] F. J. G. Cuisinier, P. Steuer, J. C. Voegel, F. Apfelbaum, I. Mayer, *J. Mater. Sci. Mater. Med.* **1995**, *6*, 85−89.
[9] J. D. Layani, F. J. G. Cuisinier, P. Steuer, H. Cohen, J. C. Voegel, I. Mayer, *J. Biomed. Mater. Res.* **2000**, *50*, 199−207.
[10] F. Apfelbaum, I. Mayer, J. D. B. Featherstone, *J. Inorg. Biochem.* **1990**, *38*, 1−8.
[11] B. Sutter, T. Wasowicz, T. Howard, L. R. Hossner, D. W. Ming, *Soil Science Society of America Journal* **2002**, *66*, 1359−1366.
[12] J. D. B. Featherstone, I. Mayer, F. C. M. Driessens, R. M. H. Verbeeck, M. Heijligers, *Calcif. Tissue Int.* **1983**, *35*, 169−171.
[13] J. D. B. Featherstone, S. Pearson, R. Z. LeGeros, *Caries Res.* **1984**, *18*, 63−66.

Received August 19, 2002
[I02466]